

Skyrmions and multi-sublattice helical states in a frustrated chiral magnet

H. Y. Yuan,^{1,*} O. Gomonay,^{1,2} and Mathias Kläui¹

¹*Institut für Physik, Johannes Gutenberg-Universität Mainz, 55099 Mainz, Germany*

²*National Technical University of Ukraine “KPI”, 03056 Kyiv, Ukraine*

(Dated: October 18, 2016)

We investigate the existence and stability of skyrmions in a frustrated chiral ferromagnet by considering the competition between ferromagnetic (FM) nearest-neighbour (NN) interaction (J_1) and antiferromagnetic (AFM) next-nearest-neighbour (NNN) interaction (J_2). Contrary to the general wisdom that long-range ferromagnetic order is not energy preferable under frustration, the skyrmion lattice not only exists but is even stable for a large field range when $J_2 \leq J_1$ compared with frustration-free systems. We defend that the enlargement of stability window of skyrmions is a consequence of the reduced effective exchange interaction caused by the frustration. A multi-sublattice helical state is found below the skyrmion phase, which results from the competition between AFM coupling that favors a two-sublattice Néel state and the chiral interaction that prefers a helix. As a byproduct, the hysteresis loop of the frustrated chiral system shrinks as the magnetization goes to zero and then opens up again, known as wasp-waist hysteresis loop. The critical field that separates the narrow and wide part of the wasp-waist loop depends exponentially on the strength of NNN coupling. By measuring the critical field, it is possible to determine the strength of NNN coupling.

I. INTRODUCTION

Frustration in spin systems refers to competing interactions that cannot be satisfied simultaneously and this phenomenon has attracted significant scientific attention in last few decades due to its unusual ordering properties of the ground states.^{1–5} One type of frustration is geometric frustration, where the frustration is caused by the special structure of the crystal lattice.^{1,6} A well-known example is the antiferromagnetically coupled Ising spin model with $S = 1/2$ on a two-dimensional (2D) triangle lattice.¹ With two spins on the vertices aligned antiparallel to each other, the third spin cannot find an preferable orientation to gain exchange energy, which results in the absence of long-range ferromagnetic order and high degeneracy of the ground states. The other type of frustration comes from the competing magnetic exchange interactions instead of the lattice itself.^{7–11} Typical examples are 2D square lattices with competing nearest-neighbor (NN) interaction J_1 and next-nearest-neighbor (NNN) interaction J_2 .¹⁰ Depending on the sign of J_1, J_2 and the ratio of J_2/J_1 , the ground state of the system could be a columnar antiferromagnet (AFM) (2-sublattice AFM), a Néel AFM (4-sublattice AFM), and a disordered phase.¹² Generally, the existence of frustration would suppress the formation of long-range ordering phase and give rise to some short-range ordered phase such as spin glass and spin liquid.^{4,5}

The skyrmion lattice, a long-range ordered vortex-like topological magnetic structure, has been recently realized in chiral magnets^{13–27} with Dzyaloshinskii-Moriya (DM) interaction.^{28,29} Each skyrmion consists of spins that point in all directions wrapping a unit sphere. Skyrmion can be represented by a topological charge $q = 1/4\pi \int dx dy \mathbf{S} \cdot (\partial_x \mathbf{S} \times \partial_y \mathbf{S}) = \pm 1$, where \mathbf{S} is the unit vector of spin and the Cartesian coordinates $x - y$ lie in the film plane. Then skyrmion lattice could be viewed as regularly patterned topological charges, whose stabil-

ity is topologically protected. An interesting question is how topologically non-trivial structures like skyrmions respond to the frustration in a system? A pioneering work studied the isotropic Heisenberg model on a triangular lattice and found that a skyrmion lattice and multi- q states could exist at non-zero temperatures even in the absence of DM interaction.³⁰ A followed work focused on the anisotropic frustrated spin model and showed that multiply periodic states even exist at zero temperature.³¹ However, yet to be known is how the frustration influences the existence and energy-preferable window (EPW) of a skyrmion lattice stabilized by DM interaction. That is the motivation of the current work.

In this article, we focus on a frustrated square lattice with DM interaction. The frustration is introduced through the competing between NN FM interaction and NNN AFM interaction. The energy-preferable window of the skyrmion phase as well as hysteresis loop of the frustrated system are studied and discussed in detail. The paper is organized as follows. In Sec II, the model and numerical method are introduced. In Sec III, the phase diagram of skyrmions and wasp-waist hysteresis loop are presented, together with detailed analysis and discussions. The conclusions are given in Sec IV.

II. MODEL AND METHOD

We consider a magnetic thin film with square lattice where x -, y - and z - axes are along the length, width and thickness directions, respectively. The lateral dimensions of the film are $L \times L$. The Hamiltonian of the system is

$$\begin{aligned}
H = & -J_1 \sum_{\langle i,j \rangle} \mathbf{S}_i \cdot \mathbf{S}_j + J_2 \sum_{\langle\langle i,j \rangle\rangle} \mathbf{S}_i \cdot \mathbf{S}_j \\
& + \sum_{\langle i,j \rangle} \mathbf{D} \cdot \mathbf{S}_i \times \mathbf{S}_j - H \sum_i \mathbf{S}_i^z,
\end{aligned} \quad (1)$$

where \mathbf{S}_i labels the classical spin orientation at site i , the first and second sums are taken over all NN and NNN pairs, respectively and J_1, J_2 refer to corresponding exchange interaction strength. The third term is DM interaction which results in the formation of skyrmions in the lattice and \mathbf{D} is the DM vector. This term is one type of Lifshitz invariant that stabilizes a skyrmion state.^{32–34} The fourth term is Zeeman energy, where the external field \mathbf{H} is along the thickness direction ($+z$). A single spin flip Monte Carlo (MC) method³⁵ is used to simulate the ground states. To mimic an infinite system, periodic boundary condition in the x and y directions are used. A typical simulation begins with a completely random state at a sufficient high temperature $T = 10 J_1/k_B$, where k_B is Boltzmann constant, and then the system is annealed to target temperature after a reasonable number of temperature steps. At each temperature, 10^4 MC steps are taken before measurements are performed. If not stated differently, the grid size $L = 32$ and NN coupling is set to $J_1 = 1.0$. It corresponds to exchange integral in the order of 10 meV.³⁶

III. RESULTS AND DISCUSSIONS

In Sec A, we will first illustrate our simulation results including the phase diagram in $H - J_2$ plane, the comparison of energy between ferromagnetic (FM), skyrmion (SkX) and helical states (H), and then provide both qualitative and quantitative analyses of the results. In Sec B, we present the results on hysteresis loop and then discuss the results in detail.

A. Phase diagram

Figure 1a shows the phase diagram in the $HJ_1/D^2 - J_2/J_1$ plane. When NNN coupling is absent i.e. $J_2 = 0$, the ground state is a helical state for $HJ_1/D^2 < 0.24$ as shown in the left panel of Fig. 1b. The chirality of the helix is counterclockwise, which is uniquely determined by the sign of the DM interaction.³⁷ For $0.24 \leq HJ_1/D^2 < 0.73$, the ground state is a triangular skyrmion lattice as shown in the left panel of Fig. 1c. It should be mentioned that the number of skyrmions decreases and the hexagonal structure of skyrmion lattice becomes irregular when the reduced field is close to 0.73. This observation may be related strip-out instability of skyrmion lattice.³⁴ As the field increases further, the ground state is a ferromagnetic single domain, where

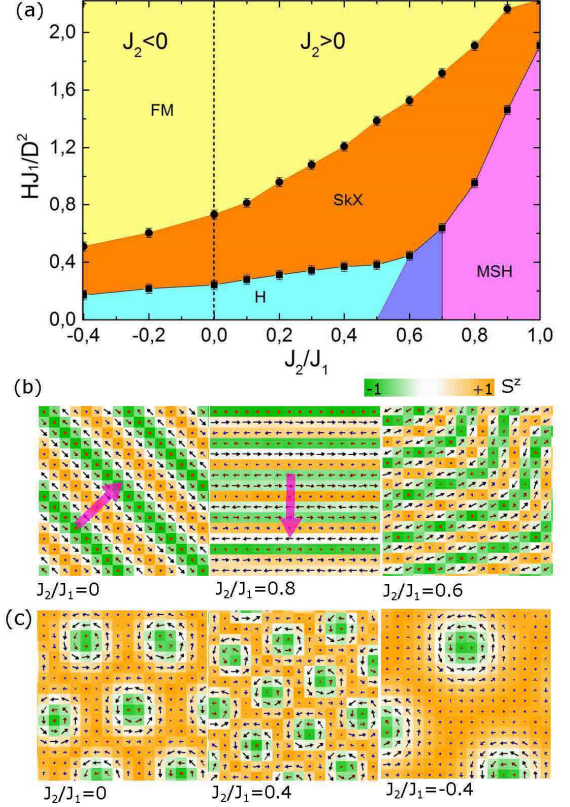


FIG. 1. (Color online) (a) The $HJ_1/D^2 - J_2/J_1$ phase diagram when NNN coupling is included. $T = 6.6 \times 10^{-3} J_1/k_B$. The color represents various phases including yellow (FM), orange (SkX), light blue (H), dark blue (Transition) and pink (MSH). The dashed line refers to $J_2 = 0$. (b) Ground states of the system for $J_2/J_1 = 0, 0.8, 0.6$ under zero field. The pink arrows indicate the direction of period. (c) Snapshot of skyrmions for $J_2/J_1 = 0, 0.4, -0.4$ under field $HJ_1/D^2 = 0.45$. The color codes S_z from -1 (green), 0 (white) to +1 (orange) as indicated in the color bar.

all the spins align in the $+z$ direction. Now, the anti-ferromagnetic NNN coupling ($J_2 > 0$) is turned on. As J_2/J_1 increases, the EPW of skyrmion phase first enlarges and then shrinks as shown in the orange region of Fig. 1a. Up to $J_2/J_1 = 0.9$, the EPW is wider than the case of $J_2 = 0$ and the maximum enlargement ratio is 2.2 around $J_2/J_1 = 0.6$. As a comparison, we simulate the case when NNN coupling is ferromagnetic ($J_2 < 0$) and find that stability region of skyrmion shrinks. The phase above the upper boundary of skyrmion phase (yellow) is always a FM state while the phase below depends on the strength of J_2/J_1 . For $J_2/J_1 \leq 0.5$, the helical state is stable. As $J_2/J_1 > 0.7$, a multi-sublattice helical (MSH) phase as shown in the middle panel of Fig. 1b, becomes stable. In the intermediate regime, it is the transition state as shown in the right panel of Fig. 1b.

A consistency check is performed by comparing the energy of skyrmions and helical states as shown in Fig.

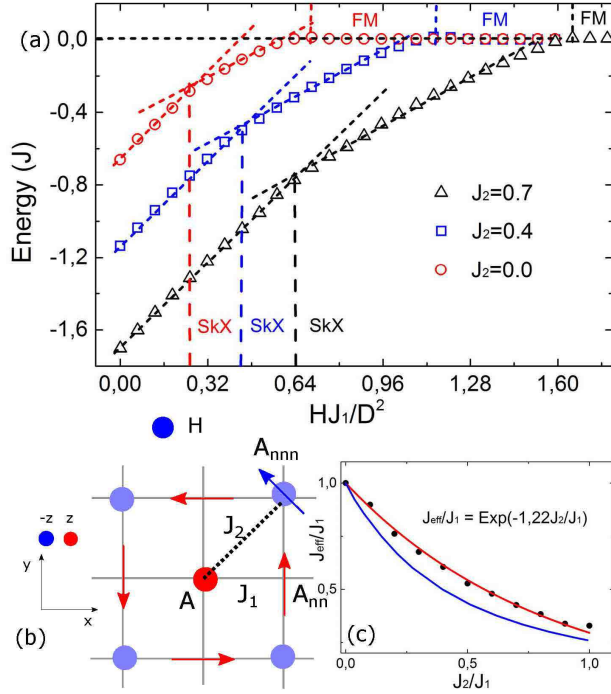


FIG. 2. (Color online) (a) Energy of the system as a function of external field for $J_2 = 0.0$ (red circles), 0.4 (blue squares) and 0.7 (black triangles). The energy is biased by the energy of a FM state. The dashed lines indicate the corresponding phase boundaries. (b) Scheme of a site A and its neighbours A_{nn} , A_{nnn} on a square lattice. (c) Effective NN exchange J_{eff} as a function of NNN exchange strength. The red line is the fitting curve using relation $J_{\text{eff}}/J_1 = \text{Exp}(-1.22J_2/J_1)$. The blue line is the theoretical prediction.

2a. The energy curve shows that the normal helical or multi-sublattice helical state has the lowest energy when the field is small, regardless of the magnitude of J_2 (red circles, blue squares and black triangles for $J_2 = 0.0, 0.4, 0.7$, respectively). the FM state is energy preferable in the large field limit. In the intermediate field regime, the skyrmion phase is energy preferable and the EPW of skyrmions (the horizontal window between two dashed lines with the same color) increases as NNN coupling increases from 0 to 0.7. As a short summary, both the phase diagram and energy comparison between various states explicitly show that a skyrmion lattice could exist and the energy-preferable window of skyrmions becomes even larger for $0 < J_2/J_1 < 1.0$. Moreover, the energy changes are continuous while the first order derivative of energy with respect to field is not continuous at the transition fields, as shown by the dashed lines connecting the discrete symbols in Fig. 2a. This indicates that the transition between the helical state and the skyrmion, the skyrmion and the FM state may be both the first order transitions.

Now we provide a qualitative understanding on the phase diagram and energy landscape. Firstly, as shown in Fig. 2b, one spin A has four nearest spins A_{nn} and

another four NNN spins A_{nnn} . The introduction of an antiferromagnetic NNN coupling would prefer the spin A_{nnn} to tilt antiparallel to the central spin A. Even though this trend would be suppressed by the ferromagnetic NN coupling of A_{nn} , it would weaken the NN coupling strength effectively. As a result, the effect of the DM interaction would be more pronounced and make the skyrmion more energetically favorable. On the other hand, the reduction of effective exchange coupling would lead to a reduction of skyrmion size,³⁸ which is consistent with our observation as shown in Fig. 1c. If it is assumed that the phase boundary between SkX and FM in Fig. 1a still follows the theoretical relation $H_c J_{\text{eff}}/D^2 = 0.73$ ³⁸ in a frustration-free system, the effective coupling J_{eff} as a function of J_2 could be extracted as shown by the black dots in Fig. 2c. An exponential fitting $J_{\text{eff}}/J_1 = \text{Exp}(-1.22J_2/J_1)$ describes the NNN coupling strength J_2 dependence of J_{eff} well.

However, the effective ferromagnetic coupling cannot capture the full physics in a frustrated system. As shown in Fig. 3a, the effective exchange cannot fully explain the phase boundary between the MSH state and the SkX state for $J_2/J_1 > 0.5$. This may be attributed to the speciality of the MSH state compared with the conventional helical state. Next, we discuss the properties of MSH in detail. For the typical example shown in the middle panel of Fig. 1b, Figure 3b shows the z component of spin (S_z) as a function of spin position in y direction. Although it shows a periodic behavior with a period of $L_H = 32a$ (a is the lattice constant), it is difficult to recognize the multi-sublattice chiral structure from this plot directly. Here we introduce a unit cell containing three sublattices with site number $3n - 2, 3n - 1, 3n$, respectively, where n is a positive integer. Figure 3c shows the space variation of spins of the three sublattices, respectively. A cosine/sine curve with period $L_H = 48a$ is observed for all the three sublattices and a constant phase lag exists for adjacent sublattices. If we only plot the spin configuration of one sublattice, it shows a regular helical structure as shown in Fig. 3d for $3n - 2$ sites. The chirality of the helix in $+y$ direction is counterclockwise, which is the same as the helical states at small J_2 . This multi-sublattice helical state is the competing result between DM interaction and exchange coupling. Specifically, when $J_2/J_1 < 0.5$, the NNN coupling is weak, hence ferromagnetic NN coupling and DM interaction dominate the other interactions in the system and the ground state is a helical state. When $J_2/J_1 > 0.5$, the AFM NNN coupling begins to surpass the NN coupling and compete with the DM interaction. Without DM interaction, the ground state is a 2-sublattice AFM state,¹⁰ where spins in a row/column would align ferromagnetically with each other and the spins in a column/row align antiferromagnetically. Once DM interaction appears, it will prefer a chiral rotation of spins in a particular direction. As a result of this balance, the spins keep their ferromagnetic order in the x direction and change the 2-sublattice AFM to a three sublattices helical state in y direction. The multi-sublattice state is

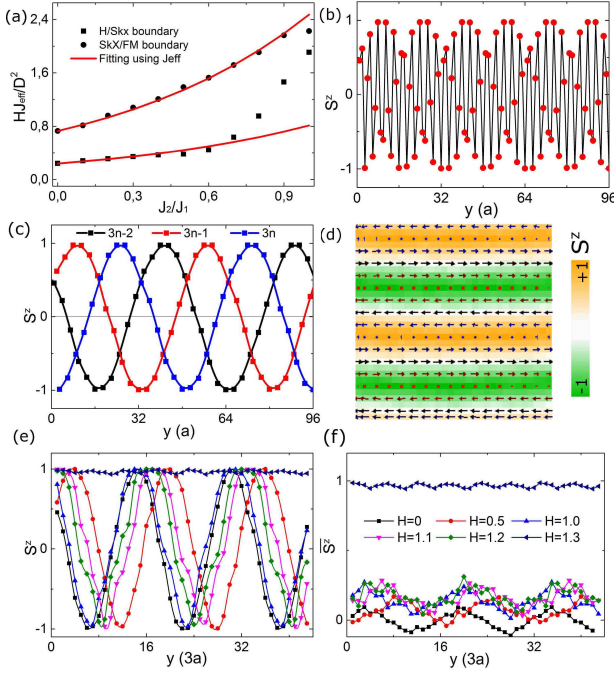


FIG. 3. (Color online) (a) Calculated phase boundary using effective NN coupling J_{eff} (red line) for H/SkX ($0.24HJ_{\text{eff}}/D^2$) and SkX/FM ($0.73HJ_{\text{eff}}/D^2$). (b) S^z as a function of the spin position (y), where a is lattice constant. (c) Re-plot of $S^z - y$ when the sites are classified into three classes $i = 3n - 2, 3n - 1, 3n$, where n is a positive integer. $y = ia$, where a is lattice constant. Black, red, blue squares represent $3n - 2, 3n - 1, 3n$, respectively. (d) A typical spin configuration of the $3n - 2$ sites. (e) $S^z - y$ for $3n - 2$ sites at various fields. (f) The average magnetization of the $3n - 2, 3n - 1$ and $3n$ sites \bar{S}^z as a function of unit cell coordinates (y) for various fields. $\bar{S}^z = (S^z_{3n-2} + S^z_{3n-1} + S^z_{3n})/3$.

very stable as it gains from both the AFM interaction and DM interaction. It should be pointed out that the multi-sublattice ordering is also possible in the x direction, since there is no anisotropy in our 2D square lattice. Figure 3e shows the $S_z - y$ for the $3n - 2$ sublattice as we increases the fields from 0 to 1.3 at the phase boundary. It shows that the sublattice chiral state is stable as the field increases up to 1.2. This special stability widens the window of multi-sublattice state and shrinks the window of skyrmions, as shown in the phase diagram of Fig. 1a. The phase difference of the $S^z - y$ curves between various fields in Fig. 3e is randomly distributed, which is related to the stochastic nature of spin flip in the annealing process. Nevertheless, as the field increases, the phase difference of the three sites within a unit cell keeps adjusting to increase the average magnetization to gain Zeeman energy, as shown in Fig. 3f.

To justify the results theoretically, we model a frustrated spin chain and study the influence of frustration

on the chiral states. The Hamiltonian is

$$H = \sum_i (-J_1 \mathbf{S}_i \cdot \mathbf{S}_{i+1} + J_2 \mathbf{S}_i \cdot \mathbf{S}_{i+2} - D e_y \cdot \mathbf{S}_i \times \mathbf{S}_{i+2} - H S_i^z).$$

The energy of FM is $E_{\text{FM}}/J_1 = -1 + J_2/J_1 - H/J_1$. For the helical state, it is assumed that the spin rotates in the xz plane such that $\mathbf{S}_n = (\sin nqa, 0, \cos nqa)$, where a is lattice constant, and the wavevector $q = 2\pi/L_H$, where L_H is the period of the helix. Substituting this trial function \mathbf{S}_n into the Hamiltonian and minimizing the total energy gives a quartic polynomial equation,

$$Dx^4 + (2J_1 + 4J_2)x^3 + (2J_1 - 4J_2)x - D = 0$$

where $x = \tan(qa/2)$. For $J_2 = 0$, the solution is $J_1 \tan(qa) = D$, which is consistent with the literature.³⁹ For $J_2 \neq 0$, the quartic solution has a positive real root (q_0), which indicates the existence of a helical structure. Substituting this root (q_0) back to the Hamiltonian, we could calculate the energy of the helix. Figure 4a shows the energy difference between the helical state and FM state as a function of J_2/J_1 . For $H/J_1 < 0.6$, the energy of helix is always smaller than the energy of FM state. For $H/J_1 > 0.6$, the helix is energetically preferred in the larger J_2/J_1 regime while FM is energetically preferred in the smaller J_2/J_1 regime. The phase diagram in the $J_2/J_1 - HJ_1/D^2$ plane is shown in Fig. 4b. By fitting the phase boundary between helix and FM state using HJ_{eff}/D^2 , we could extract the effective exchange as a function of J_2/J_1 in the frustrated system, as shown in the blue line of Fig. 2c. The theoretical curve captures the trend of numerical results (black dots) in the 2D square lattice.

B. Hysteresis loop

In this section, we investigate the shape of hysteresis loop in a frustrated system. The thermal effect is suppressed by considering a system at sufficiently low temperature $T = 6.67 \times 10^{-3} J_1/k_B$. Figure 5a,b shows the first magnetization curve. The average magnetization is defined as $\langle S_z \rangle = 1/L^2 \sum_i S_i^z$. To simulate the first magnetization, we start from a helical state obtained from an annealing process under $H = 0$ and then increase the field in the step of $0.1J_1/D^2$. For $J_2 = 0$, the helical phase is stable up to $HJ_1/D^2 = 0.76$ and skyrmion phase only exists in a narrow window for $0.76 < HJ_1/D^2 < 0.95$, as shown in Fig. 3a. For $J_2 = 0.4$, skyrmion is stable at the range $0.70 < HJ_1/D^2 < 1.52$, which is significantly larger than the window at $J_2 = 0$. For both $J_2 = 0$ and $J_2 = 0.4$, the existence regime of the skyrmion phase is different from the phase diagram shown in Fig. 1a, which is due to the hysteretic nature of a magnetic system.²² The final spin configuration depends sensitively on the evolution history, even though the initial states

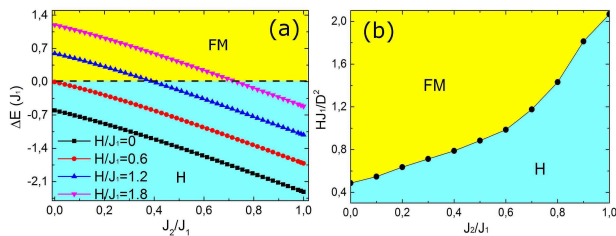


FIG. 4. (Color online) (a) Energy density difference between a helical state and a FM state calculated from 1D frustrated model under fields $H/J_1 = 0$ (black square), 0.6 (red dots), 1.2 (blue up-triangles), 1.8 (pink down-triangles). The light blue/yellow region refers to the region with FM and helix as ground states, respectively. (b) The calculated phase diagram in $HJ_1/D^2 - J_2/J_1$ plane. The yellow and light blue color represent FM and H states, respectively.

are the same. The annealing procedure is more efficient to reach the real global minimum states of the system because sufficient energy is provided to the spins to overcome the energy barrier between skyrmion and H/FM. Under a fixed low temperature ($6.67 \times 10^{-3} J_1/k_B$), the thermal energy is too small for the system to overcome the energy barrier to reach a skyrmion state unless sufficient large field is applied such that the energy barrier is substantially lowered.

Figure 5c and 5d show the hysteresis loop for $J_2 = 0$ and $J_2 = 0.4$, respectively. To simulate the hysteresis loop, we start from a FM state obtained by annealing procedures at high fields and then decrease the fields in the step of $0.1J_1/D^2$ to obtain the descending branch and then reverse the direction of fields to get the ascending branch. Both the hysteresis loops in Fig. 5c and 5d take on a wasp-waist shape, where the loop shrinks as magnetization goes to zero and then opens up again. The field that separates the wide and narrow part of the hysteresis loop is denoted as the critical field (H_c). The critical field is $H_c = 0$ for $J_2 = 0$ while it is at $H_c = 0.13D^2/J_1$ for $J_2 = 0.4$, as shown in Fig. 5c and 5d. To see clearly the loop in the small magnetization regime and understand the role of finite size effect in the simulations, we vary the system size as $L = 32, 64, 96, 128, 192$ and plot all the loops in Fig. 5e. For $L = 32$ (black dots), a quasi-closed loop exists, and it disappears as L increases. The L dependence of the magnetization for the ascending branch and descending branch at zero field is plotted in Fig. 5f. The gap between the two branches decreases gradually to a constant. It is expected that the loop at smaller fields would result in two closely parallel branches as $L \rightarrow \infty$.

To understand the wasp-waist hysteresis, we refer to the scheme in Fig. 2b. As we reduce the fields slowly from a high field value, the system first stabilizes at a FM state, where spins at A and its neighbors A_{nn} and A_{nnn} (almost) align in the $+z$ direction. Similar to the argument for the first magnetization curve, even though the skyrmion/helical states are the global minimum states

for $HJ_1/D^2 < 0.76$, however the FM state ($q = 0$) and skyrmions ($q = \pm 1$) are topologically different, where the transformation between them needs to overcome a finite energy barrier. As the temperature is low, the degree of freedom for the spins frozen and the system always tends to evolve to a lower energy state, which makes it difficult to climb across the barrier. The system finally evolves to a helical state ($q = 0$) at zero field. When antiferromagnetic NNN coupling is present, the spins between A_{nn} and A will tend to align antiparallel to each other, which will destabilize the FM state and lower the energy barrier between FM and helical states. That's why the critical field becomes finite. According to this argument, the larger the NNN coupling (J_2), the lower the barrier between the FM and helical states, hence the larger the critical field. This is demonstrated by the simulations as shown in the inset of Fig. 5g. The critical field increases almost exponentially with the increase of J_2 . This may provide a method to measure the strength of NNN coupling in a ferromagnetic film by measuring the critical field in the corresponding wasp-waist hysteresis loop.

Lastly, we would like to mention that a similar wasp-waist hysteresis loop was experimentally observed in Co/Pt multi-layer structures with low disorder.⁴⁰ At the critical field that magnetization decreases significantly, a labyrinth-like magnetic pattern was observed. Another system that allows for the wasp-waist loop is a chiral system with in-plane easy-axis anisotropy.⁴¹ The critical field of the hysteresis loop depends on the in-plane anisotropy strength. One should be careful to clarify the source of the critical field when NNN coupling and easy-axis anisotropy are possible to coexist in a system. Moreover, it is known that the exchange coupling of Fe could be both ferromagnetic and antiferromagnetic which depends on the substrates' d-band filling.⁴²⁻⁴⁴ Recently, *ab initio* calculation showed that ferromagnetic NN and AFM NNN interaction could coexist in multi-layer $Pt_{1-x}Ir_x$ /Fe/Pd structures,⁴⁵ where our simulation results are promising and remain to be verified experimentally.

IV. CONCLUSIONS

In conclusion, we have studied the existence and the energy-preferable window of skyrmions in a frustrated magnet. The AFM NNN interaction diminishes the FM NN interaction to a certain degree and the DM interaction becomes more pronounced, hence the skyrmions could be stabilized in an even larger window compared to a system without frustration. The theory based on the effective ferromagnetic exchange could quantitatively capture the phase boundary among skyrmions, FM states and the helix, except for the skyrmion/helix boundary when the AFM coupling is larger than half of the FM coupling. In this regime, a multi-sublattice state instead of a conventional helical state exists below the skyrmion phase. The multi-sublattice state gains both AFM and

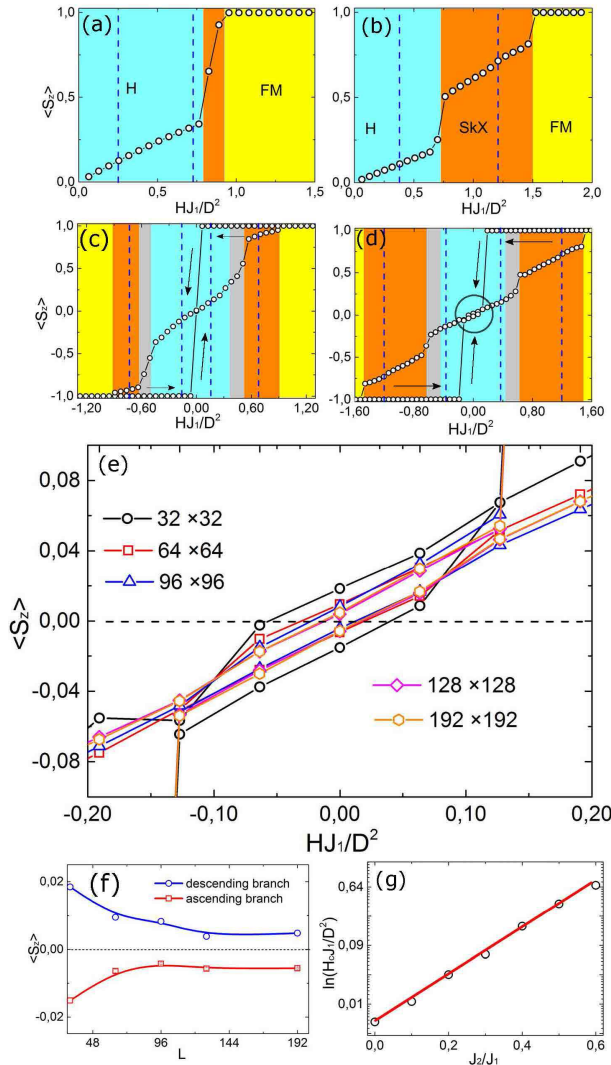


FIG. 5. (Color online) First magnetization curve for $J_2 = 0$ (a) and $J_2 = 0.4$ (b), and hysteresis loop for $J_2/J_1 = 0.0$ (c) and 0.4 (d). $\langle S_z \rangle$ is defined as $\langle S_z \rangle = 1/L^2 \sum_i S_i^z$. Blue: helix, orange: skyrmion, yellow: FM state, gray: mixing of helix and skyrmion. (e) is the enlarged figure of the circle in (d). $T = 6.6 \times 10^{-3} J_1/k_B$, $L = 32$. (e) Size effect of the hysteresis loop at small fields for $L = 32$ (black circles), 64 (red squares), 96 (blue triangles), 128 (pink diamonds), 192 (yellow hexagons), respectively. (f) $\langle S_z \rangle$ as a function of sample size for descending branch (blue circles) and ascending branch (red squares), respectively. (g) The critical field H_c as a function of J_2/J_1 .

DM energy and is energetically preferable up to high fields. Moreover, the hysteresis loop of the frustrated system takes on wasp-waist shape and the critical field at which the loop shrinks depends on the strength of NNN coupling. By measuring the critical field, it is possible to determine the strength of NNN coupling.

ACKNOWLEDGMENTS

We acknowledge the support from Deutsche Forschungsgemeinschaft (DFG) via the Transregional Collaborative Research Center (SFB/TRR) 173 “Spin+X - Spin its collective environment” and the ERC Synergy Grant SC2 (No. 610115).

* Corresponding author: huaiyangyuan@gmail.com

¹ G. H. Wannier, Phys. Rev. **79**, 357 (1950).

² J. Stephenson, J. Math. Phys. **11**, 413 (1970).

³ L. G. Marland and D. D. Betts, Phys. Rev. Lett. **43**, 1968 (1979).

⁴ L. Balents, Nature **464**, 199 (2010).

⁵ K. Binder and A. P. Young, Rev. Mod. Phys. **58**, 801 (1986).

⁶ J. T. Chalker, P. C. W. Holdsworth, and E. F. Shender, Phys. Rev. Lett. **68**, 855 (1992).

⁷ J. Villain, J. Phys. C: Solid State Phys. **10**, 1717 (1977).

⁸ J. Vannimenus and G. Toulouse, J. Phys. C: Solid State Phys. **10**, L537 (1977).

⁹ P. Chandra and B. Doucot, Phys. Rev. B **38**, 9335 (1988).

¹⁰ A. A. Tsirlin, R. Nath, A. M. Abakumov, R. V. Shpanchenko, C. Geibel, and H. Rosner, Phys. Rev. B **81**,

- 174424 (2010).
- ¹¹ R. Nath, A. A. Tsirlin, E. E. Kaul, M. Baenitz, N. Büttgen, C. Geibel, and H. Rosner, *Phys. Rev. B* **78**, 024418 (2008).
 - ¹² N. Shannon, T. Momoi, and P. Sindzingre, *Phys. Rev. Lett.* **96**, 027213 (2006).
 - ¹³ A. N. Bogdanov and U. K. Rößler, *Phys. Rev. Lett.* **87**, 037203 (2001).
 - ¹⁴ U. K. Rößler, A. N. Bogdanov, and C. Pfleiderer, *Nature* **442**, 797 (2006).
 - ¹⁵ S. Mühlbauer, B. Binz, F. Jonietz, C. Pfleiderer, A. Rosch, A. Neubauer, R. Georgii, and P. Böni, *Science* **323**, 915 (2009).
 - ¹⁶ X. Z. Yu, Y. Onose, N. Kanazawa, J. H. Park, J. H. Han, Y. Matsui, N. Nagaosa, and Y. Tokura, *Nature* **465**, 901 (2010).
 - ¹⁷ W. Münzer et al., *Phys. Rev. B* **81**, 041203 (2010).
 - ¹⁸ X. Z. Yu et al., *Nat. Mater.* **10**, 106 (2011).
 - ¹⁹ S. Heinze, K. von Bergmann, M. Menzel, J. Brede, A. Kubetzka, R. Wiesendanger, G. Bihlmayer, and S. Blügel, *Nat. Phys.* **7**, 713 (2011).
 - ²⁰ Y. Onose, Y. Okamura, S. Seki, S. Ishiwata, and Y. Tokura, *Phys. Rev. Lett.* **109**, 037603 (2012).
 - ²¹ T. Schulz et al., *Nat. Phys.* **8**, 301 (2012).
 - ²² S. Buhrandt and L. Fritz, *Phys. Rev. B* **88**, 195137 (2013).
 - ²³ A. Fert, V. Cros, and J. Sampaio, *Nat. Nanotech.* **8**, 152 (2013).
 - ²⁴ J. Iwasaki, M. Mochizuki, and N. Nagaosa, *Nat. Commun.* **4**, 1463 (2013).
 - ²⁵ S. M. Mohseni, S. R. Sani, J. Persson, T. N. Anh Nguyen, S. Chung, Ye. Pogoryelov, P. K. Muduli, E. Iacocca, A. Eklund, R. K. Dumas, S. Bonetti, A. Deac, M. A. Hofer, and J. Åkerman, *Science* **339**, 1295 (2013).
 - ²⁶ H. S. Park, X. Yu, S. Aizawa, T. Tanigaki, T. Akashi, Y. Takahashi, T. Matsuda, N. Kanazawa, Y. Onose, D. Shindo, A. Tonomura, and Y. Tokura, *Nat. Nanotech.* **9**, 337 (2014).
 - ²⁷ S. Woo et al., *Nat. Mater.* **15**, 501 (2016).
 - ²⁸ I. E. Dzyaloshinskii, *Sov. Phys. JETP* **5**, 1259 (1957).
 - ²⁹ T. Moriya, *Phys. Rev.* **120**, 91 (1960).
 - ³⁰ T. Okubo, S. Chung, and H. Kawamura, *Phys. Rev. Lett.* **108**, 017206 (2012).
 - ³¹ A. O. Leonov and M. Mostovoy, *Nat. Commun.* **6**, 8275 (2015).
 - ³² Y. A. Izyumov, *Usp. Fiz. Nauk* **144**, 439 (*Sov. Phys. Usp.* **27**, 11) (1984).
 - ³³ A. N. Bogdanov and D. A. Yablonskiĭ, *Zh. Eksp. Teor. Fiz.* **95**, 178 (*Sov. Phys. JETP* **68**, 101) (1989).
 - ³⁴ A. O. Leonov, T. L. Monchesky, N. Romming, A. Kubetzka, A. N. Bogdanov, and R. Wiesendanger, *New J. Phys.* **18**, 065003 (2016).
 - ³⁵ N. Metropolis, A. W. Rosenbluth, M. N. Rosenbluth, A. H. Teller, and E. Teller, *J. Chem. Phys.* **21**, 1087 (1953).
 - ³⁶ C. Kittel, *Introduction to Solid State Physics*, 7th Ed. (Wiley, New York, 1996).
 - ³⁷ H. Y. Yuan and X. R. Wang, *Sci. Rep.* **6**, 22638 (2016).
 - ³⁸ J. H. Han, J. Zang, Z. Yang, J. -H. Park, and N. Nagaosa, *Phys. Rev. B* **82**, 094429 (2010).
 - ³⁹ S. D. Yi, S. Onoda, N. Nagaosa, and J. H. Han, *Phys. Rev. B* **80**, 054416 (2009).
 - ⁴⁰ M. S. Pierce, C. R. Buechler, L. B. Sorensen, S. D. Kevan, E. A. Jagla, J. M. Deutsch, T. Mai, O. Narayan, J. E. Davies, K. Liu, G. T. Zimanyi, H. G. Katzgraber, O. Hellwig, E. E. Fullerton, P. Fischer, and J. B. Kortright, *Phys. Rev. B* **75**, 144406 (2007).
 - ⁴¹ H. Y. Kwon, K. M. Bu, Y. Z. Wu, C. Won, *J. Magn. Magn. Mater.* **324**, 2176 (2012).
 - ⁴² B. Hardrat, A. Al-Zubi, P. Ferriani, S. Blügel, G. Bihlmayer, and S. Heinze, *Phys. Rev. B* **79**, 094411 (2009).
 - ⁴³ L. Rózsa, L. Udvardi, L. Szunyogh, and I. A. Szabó, *Phys. Rev. B* **91**, 144424 (2015).
 - ⁴⁴ L. Rózsa, E. Simon, K. Palotás, L. Udvardi, and L. Szunyogh, *Phys. Rev. B* **93**, 024417 (2016).
 - ⁴⁵ L. Rózsa, A. Deak, E. Simon, R. Yanes, L. Udvardi, L. Szunyogh, and U. Nowak, *arXiv:1606.02464v1*.